

Hierarchical Target Learning in the Mammalian Neocortex: A Pyramidal Neuron Perspective

Pau Vilimelis Aceituno^{*,1,3}, Sander de Haan^{*,1,2,3},
Reinhard Loidl¹, and Benjamin F. Grawe^{1,3,†}

¹Institute of Neuroinformatics, University of Zurich and ETH Zurich

²Institute of Social Ethics, University of Lucerne

³ETH AI Center, ETH Zurich

†Correspondence: bgrewe@ethz.ch

*Equal contribution

April 10, 2024

1 Abstract

The mammalian neocortex possesses the remarkable ability to translate complex sensory inputs into abstract representations through the coordinated activity of large neuronal ensembles across the sensory hierarchy. While cortical hierarchies are anatomically well described, how learning is orchestrated across the spatial scales ranging from large neuronal networks to pyramidal neurons and their individual synapses is unknown. Here we address this gap from the ground up by modeling the membrane potential and calcium dynamics of individual pyramidal neuron synapses while working upward toward network learning. Starting at the lowest level, we adopt a calcium-dependent synaptic plasticity rule consistent with a wide range of molecular and electrophysiological findings and implement this rule in a synaptic model. We then embed our synaptic model into a pyramidal cell model with apical and dendritic compartments, and integrate various experimental observations such as bursts, calcium plateaus, and somato-apical coupling. We validate the predictions of our neuron model through direct *in vitro* electrophysiology experiments on layer 5 (L5) pyramidal neurons from the mouse prefrontal cortex and demonstrate that inputs arriving at apical dendrites guide plasticity at basal synapses. Finally, we investigate the algorithmic principles of hierarchical credit assignment in the mammalian neocortex by embedding our pyramidal neuron model in various biologically-plausible deep learning architectures that have been proposed to explain learning in cortex. We find that our model seamlessly aligns with target learning architectures, where top-down feedback arriving at the apical dendrite modifies pyramidal neuron activities to align with desired higher-level neural activity. Importantly, supported by our biological data, this cortical target learning cannot be easily cast into the backpropagation algorithm. By providing a cross-scale framework for cortical hierarchical learning, our work reveals a potential discrepancy between learning in biological neural networks and conventional deep learning.

2 Introduction

Learning in the cortex involves a variety of mechanisms for processing and modifying information, both forward and backward, between hierarchical levels. These mechanisms operate at different spatial scales, from extensive neuronal networks to individual neurons and their synapses. At the network level, studies have shown that the response characteristics of neurons at various hierarchical stages of visual cortical processing are similar to those observed in deep artificial neural networks (Yamins and DiCarlo, 2016; Khaligh-Razavi and Kriegeskorte, 2014a). This observation motivated the development of ‘cortical-inspired’ deep network models that approximate the well-known gradient descent backpropagation (BP) training algorithm for deep learning (Scellier and Bengio, 2017; Whittington and Bogacz, 2017; Sacramento et al., 2018; Payeur et al., 2021). These models feature pyramidal neurons that modify their feedforward synaptic strength based on an explicit top-down error signal from higher cortical areas. However, this approach to understanding biological learning presents a significant challenge. While optimizing for function and enhanced deep learning performance, the structure and behavior of these network models often diverge from biology. This led to the development of a variety of models with different assumptions and working principles that do not fully explain biology and are incompatible with each other. Here, we take a different approach by starting from fundamental biological principles and focusing on the physiological behavior and plasticity of individual pyramidal neurons and their synapses. We begin by constructing a neuron model based on well-established properties of pyramidal neurons and their synapses. We then use this model to make predictions on how pyramidal neurons learn, which we verify experimentally. Finally, we investigate the algorithmic principles of hierarchical credit assignment by embedding our neuron model into a range of biologically-plausible network architectures (**Fig. 1**).

2.1 Bridging molecular mechanisms and cellular dynamics.

Molecular level studies reported that synaptic calcium plays a crucial role in driving plasticity in cortical neurons (Lisman, 1989; Yang et al., 1999; Evans and Blackwell, 2015). Calcium in the post-synaptic spine is regulated through NMDA receptors (NMDARs), which are essential for initiating plasticity (Artola and Singer, 1987; Bear et al., 1992; Markram et al., 1997; Sjöström et al., 2003). For NMDARs to open, both glutamate from presynaptic activity, as well as a second postsynaptic signal are required, which could be a backpropagating action potential (bAP) originating from the somato-axonal region (Grewe et al., 2010) or a bAP-activated calcium plateau potential originating from the apical tuft (Larkum et al., 1999). Depending on the synaptic calcium concentration, calcium-dependent plasticity pathways based on protein kinases or phosphatases are then activated, leading to long-term potentiation (LTP) or long-term depression (LTD) respectively (Lisman, 1989). This has led to the idea that the concentration and temporal dynamics of synaptic calcium dictates the direction and magnitude of synaptic plasticity (Yang et al., 1999; Evans and Blackwell, 2015). Each synapse maintains its strength when calcium concentrations are below the LTD threshold. Exceeding this threshold induces LTD until a second threshold is reached, beyond which LTP is triggered (Chindemi et al., 2022). This type of calcium-dependent learning rule aligns with both molecular studies and phenomenological learning rules such as spike-timing-dependent plasticity (STDP) (Graupner and Brunel, 2012; Chindemi et al., 2022). In STDP, a single postsynaptic bAP is thought to affect synaptic calcium shortly after an excitatory postsynaptic potential (EPSP) is generated (Markram et al., 1997). However, recent experimental data show that single bAPs show either drastically reduced or no LTP in conditions of physiologically relevant extracellular calcium concentrations (Inglebert et al., 2020; Chindemi et al., 2022). In contrast, stimulating inputs to L5 apical dendritic tuft is sufficient for LTP induction even in the absence of any bAPs (Williams

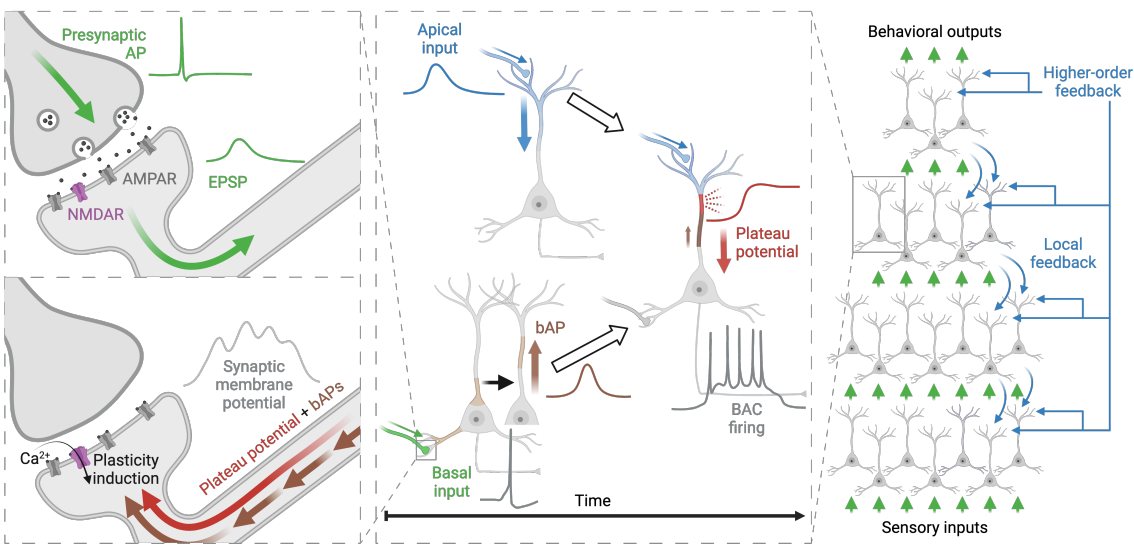


Figure 1: Organisation of cortical learning across scales. The synaptic scale (left) implements synaptic changes depending on pre- and postsynaptic activity through changes in synaptic membrane potential and its associated calcium influx. The cellular scale (middle) models the emergence of plateau potentials and BAC firing through coinciding suprathreshold basal inputs and apical input. The network scale (right) directs sensory feedforward input to activity on basal synapses and feedback signals to activity on apical synapses.

and Holtmaat, 2019). This suggests that L5 apical dendritic activity plays a major role in directing synaptic plasticity at basal dendrites.

In L5 apical dendrites, the tuft region forms a distinct integrative compartment (Larkum et al., 1999, 2001), primarily integrating synaptic inputs from higher cortical and subcortical areas (Williams and Holtmaat, 2019) as well as bAPs originating at the somato-axonic region. Typically, top-down inputs to the apical tuft either excite or suppress local dendritic activity but do not induce a calcium plateau potential or trigger somatic APs on their own (Fişek et al., 2023). Likewise, bAPs emerging from basally-induced APs are usually insufficient to initiate a calcium plateau potential (Grewe et al., 2010). However, when inputs to the apical dendrite coincide with a bAP induced by basal inputs, the resulting depolarization at the apical dendrite can cross a threshold, after which calcium plateau potentials initiate (Larkum et al., 1999). Once generated, these plateau potentials propagate towards the somato-axonic region, where the membrane depolarization facilitates short, high-frequency bursts of APs, also known as bAP activated Ca^{2+} spike firing (BAC firing).

Thus, our synaptic plasticity model starts by considering calcium dynamics and the single synapse level. Then, we integrate our synapse in a neuron model that captures both bAPs and plateau potentials, the two most prominent cellular events that have been linked to synaptic depolarization and thus can affect synaptic calcium levels.

3 Results

We start by developing a synaptic model based on well-established calcium dynamics and learning rules, similar to that used by Graupner and Brunel (2012). To link synaptic calcium to the diverse

intracellular signaling processes, we next expand the model by adding somatic and apical dendritic compartments. As observed in biology (Larkum et al., 1999, 2001), we treat the soma and apical dendrite as distinct integrative compartments that exchange information through bAPs and plateau potentials. Apical dendritic plateau potentials occur when distal apical dendritic inputs and bAPs coincide at the main bifurcation of the apical dendrite. The generation of the first bAP is mainly driven by basal synaptic inputs that are integrated at the somato-axonic region. To implement somatodendritic coupling, we link bAPs to influence the generation of plateau potentials, and plateau potentials to influence the generation of additional somatic APs, as reported by Larkum et al. (1999). This bidirectional link enables apical input to modulate the neuronal activity through the generation of plateau potentials. Through the propagation of the plateau potential and bAPs into the basal dendritic tree, we connect apical inputs to the modulation of the synaptic membrane potential of basal synapses. This, in turn, modulates synaptic calcium influx that induces plasticity. In the following section, we provide the specific equations that form the basis of our synaptic and neuron models, and demonstrate their behaviors.

3.1 Synaptic plasticity and calcium dynamics

Within the synapse, NMDARs register presynaptic activity and the local membrane potential, which in turn affect synaptic calcium levels. Following this logic, we define the change in synaptic strength as proportional to the presynaptic input v_{pre} and the synaptic calcium concentration c ,

$$\Delta w \propto \int v_{pre}(t)P(c(t))dt \quad (1)$$

where Δw is the change in synaptic strength, P is a nonlinear plasticity function analogous to the plasticity functions outlined in Graupner and Brunel (2012); Honnuraiah and Narayanan (2013) and shown in **Fig. 3F**. Given the shape of P , plasticity is induced only after the levels of calcium reach a first LTD threshold, after which the synapse depresses until a second LTP threshold is reached and the synapse potentiates. The calcium concentration then depends on the synaptic voltage acting on NMDARs.

$$\tau_c \dot{c} = -c + (1 - \frac{c}{c_{\max}})I(v_{\text{synapse}}) \quad (2)$$

where c_{\max} is the saturated calcium concentration, τ_c is the calcium time constant, and I represents the influx of calcium through NMDARs characterized by McRory et al. (2001); Slutsky et al. (2004). Next, we model the synaptic membrane potential for which we adopt classic leaky integrate-and-fire dynamics,

$$\tau_v \dot{v}_{\text{synapse}} = -v_{\text{synapse}} + \sum_{t \in \text{EPSPs}} \kappa_{\text{EPSP}}^{\text{synapse}} * \delta(t) + \sum_{t \in \text{bAPs}} \kappa_{\text{bAP}}^{\text{synapse}} * \delta(t) + \sum_{t \in \text{Plateaus}} \kappa_{\text{plateau}}^{\text{synapse}} * \delta(t) \quad (3)$$

where τ_v corresponds to the membrane voltage time constant, $\delta(t)$ stands for the Dirac delta function at time t , the $*$ denotes the convolution operator, and κ indicates the response induced by the subscripted event in the superscripted compartment. Here, the synaptic membrane potential is determined by basal EPSPs, bAPs, and plateau potentials (for an overview of all hyperparameters, see **Methods 7.6**).

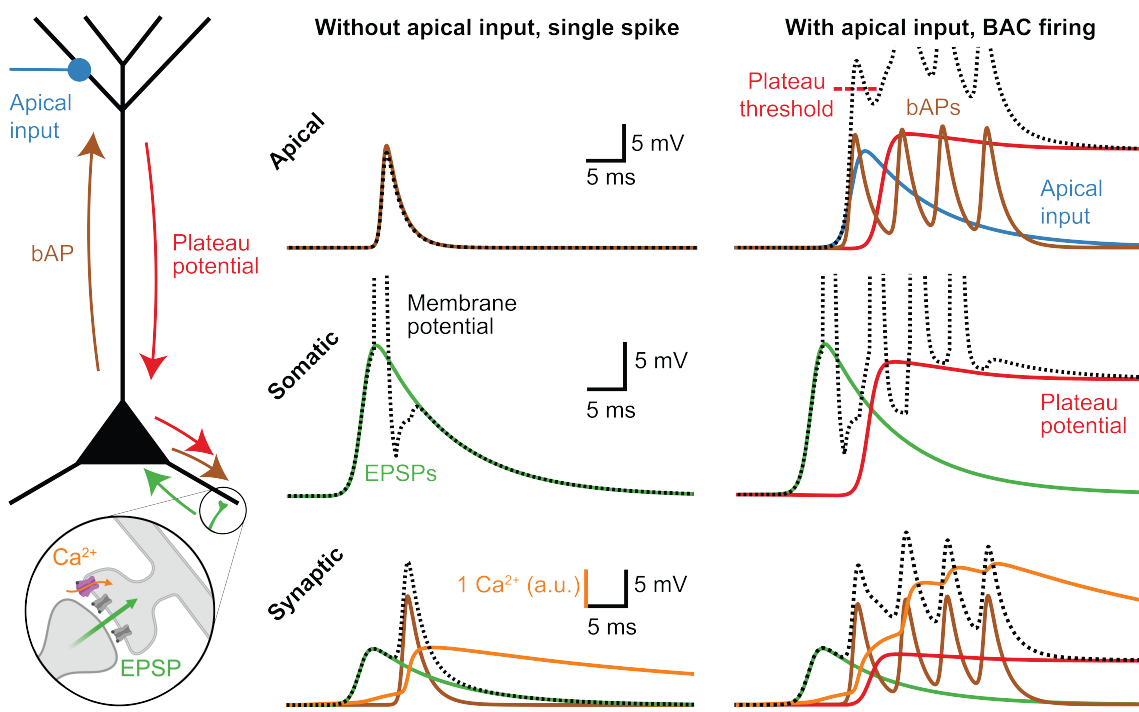


Figure 2: Pyramidal neuron simulations integrating basal and apical inputs. The neuron schematic (left) details all events and interactions inside the model. Responses of each compartment are shown for apical, somatic, and synaptic compartments for cases without (middle) and with (right) top-down input to the apical dendrite

3.2 Intracellular dynamics of pyramidal neurons

Next, we complement the synaptic model with somatic and apical compartments that feature similar integrate-and-fire dynamics. Importantly, APs are only generated in the somatic compartment, and plateau potentials are only generated in the apical compartment.

$$\tau_v \dot{v}_{\text{apical}} = -v_{\text{apical}} + \sum_{t \in \text{EPSPs}} \kappa_{\text{EPSP}}^{\text{apical}} * \delta(t) + \underbrace{\sum_{t \in \text{Plateaus}} \kappa_{\text{plateau}}^{\text{apical}} * \delta(t)}_{\text{Red bracket}} + \underbrace{\sum_{t \in \text{bAPs}} \kappa_{\text{bAP}}^{\text{apical}} * \delta(t)}_{\text{Orange bracket}} \quad (4)$$

$$\tau_v \dot{v}_{\text{soma}} = -v_{\text{soma}} + \sum_{t \in \text{Pre}} \kappa_{\text{pre}}^{\text{soma}} * \delta(t) + \underbrace{\sum_{t \in \text{Plateaus}} \kappa_{\text{plateau}}^{\text{soma}} * \delta(t)}_{\text{Red bracket}} + \underbrace{\sum_{t \in \text{APs}} \kappa_{\text{AP}}^{\text{soma}} * \delta(t)}_{\text{Orange bracket}} \quad (5)$$

The somatic membrane potential integrates EPSPs originating from presynaptic activity at basal dendrites and plateau potentials. In contrast, the membrane potential in the apical compartment is shaped by presynaptic feedback EPSPs received at the apical dendrites and bAPs. As a result, inputs received at basal synapses are integrated very differently from those at apical synapses. While basal inputs contribute to the generation of an initial somatic AP, apical synaptic inputs can be integrated with bAPs, thereby contributing to the generation of apical plateau potentials and, in turn, facilitating BAC firing (see Fig. 2).

3.3 Integration of apical feedback signals

In our neuron model, apical feedback signals can elicit a plateau potential when integrated with basally-induced bAPs. This plateau potential then subsequently propagates towards the somatoaxonic region, depolarizing the somatic membrane potential and facilitating BAC firing (**Fig. 3A**). Our model dynamics align with previous studies (Larkum et al., 2004), showing that apical input significantly modulates the firing rate of a neuron in a multiplicative manner (**Fig. 3B**). In contrast, basal inputs in the absence of apical inputs lead to the generation of singular APs without burst.

The modulation of apical input on the behavior of the neuron further affects the membrane potential and calcium dynamics at the synapse, as outlined in **Eq. 2 & 3**. The EPSPs and bAPs cause brief synaptic depolarization, while a quick succession of bAPs together with the plateau potential results in prolonged somatic as well as synaptic depolarization (**Fig. 3C**). Consequently, the membrane potential at basal synapses increases proportionally to the apical input (**Fig. 3D**). This change in synaptic membrane potential directly influences synaptic calcium influx through NMDARs, only when glutamate from a preceding EPSP is present, leading to accumulation of synaptic calcium (**Fig. 3E**). As a result, our model displays a moderate synaptic calcium influx in the absence of apical input, whereas we observe larger synaptic calcium concentrations when basal and apical inputs coincide.

3.4 Apical input possibly supervises basal plasticity in pyramidal neurons

Our neuron model describes the interplay between apical and basal inputs and the resulting effect on synaptic calcium. Still, we have not yet explored how the resulting synaptic plasticity alters sensory processing. To investigate this, we consider two distinct information pathways: sensory (bottom-up) inputs arriving at basal dendrites and (top-down) feedback from higher cortical areas arriving at the apical dendrite (Bannister, 2005; Petreanu et al., 2009; Godenzini et al., 2022). To test if and how apical inputs could instruct plasticity at basal synapses, we next adopt a simple apical feedback learning circuit (Aceituno et al., 2023). This circuit simply compares the firing rate of the neuron with its target firing rate for a specific input, and then sends the difference as a feedback input to the apical dendrite until the neuron has reached its desired and stimulus-specific target activity. Our proof-of-concept toy experiment involves two presynaptic neurons A and B , with synaptic weights w_A and w_B respectively, both connected to a single postsynaptic neuron (**Fig. 3G**). Before training, neuron A has a weak connection to the postsynaptic neuron, while neuron B is strongly connected. During training, stimuli S_A and S_B activate neurons A and B , respectively. The feedback circuit now shapes the apical input (i.e., the supervised learning signal) to invert this behavior, effectively swapping the synaptic strengths w_A and w_B .

Figure 3H shows the evolution of the two synaptic weights over learning. As the neuron increasingly aligns with its target activity, two key metrics indicate the learning progress. First, the amount of top-down apical input required to align the stimulus' response of the neuron with the target decreases over time towards a baseline (see **Methods 7.2**). Second, the Mean Squared Error (MSE), which corresponds to the squared difference between the output rate of the network and the target value, also reduces (**Fig. 3I**).

Overall, we observe that during learning, the synaptic plasticity gradually adjusts basal inputs so that the neural activity yields the desired target response without feedback (see **Methods 7.3** for an analytical proof), yielding a form of supervised target learning. In essence, our neuron model provides a possible explanation of how pyramidal cells could learn to selectively respond to specific inputs or input classes guided by top-down apical inputs.

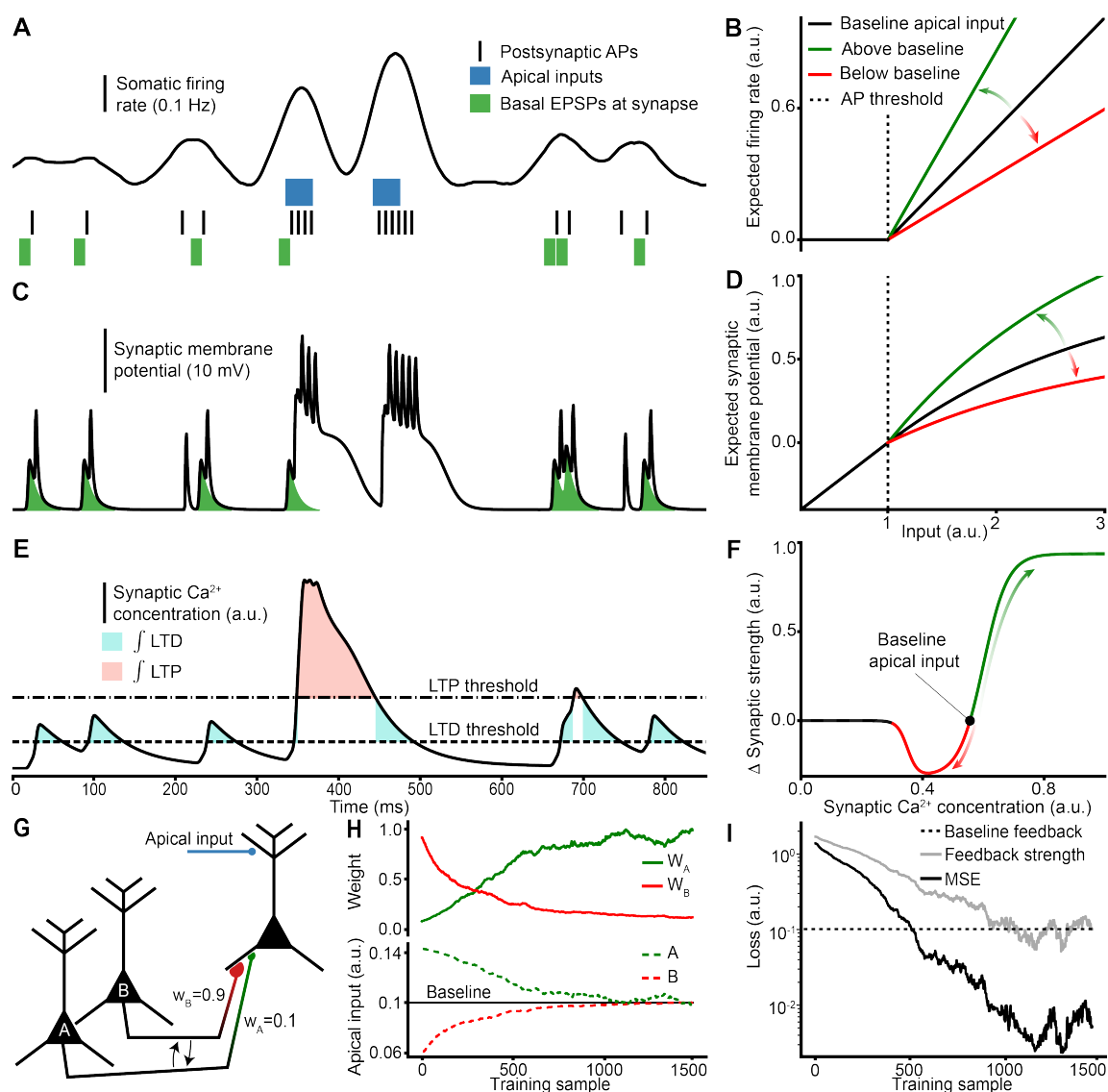


Figure 3: Effects of apical input on somatic firing rate, synaptic membrane potential, calcium influx, and plasticity. (A) Neuron firing rate with and without strong apical input. (B) The expected firing rate modulation depends on the strengths of basal and apical inputs. (C) Synaptic membrane potential integrating EPSPs, bAPs, and plateau potentials. (D) Expected synaptic membrane potential modulation integrating basal and apical inputs. (E) Synaptic calcium concentrations with LTD and LTP thresholds and their integration. (F) Synaptic plasticity as a function of synaptic calcium for various degrees of apical input modulation. (G) Schematic of the single neuron supervised learning setting, with neuron B having a higher weight than neuron A , and top-down feedback arriving at the apical dendrite. The learning objective is for the two presynaptic neurons to reverse their associations with the postsynaptic neuron. (H) Evolution of the synaptic weights (top) and the apical input (bottom). (I) Learning progress indicated by the absolute feedback strengths and the MSE loss.

3.5 The integration of basal and apical inputs directs synaptic learning in basal synapses

Our neuron model predicts that synaptic plasticity is guided primarily by synaptic membrane depolarization, where sustained somatic depolarization through plateau potentials tends to induce LTP while brief depolarization through single somatic APs tend to induce LTD. To support our predictions, we next performed *in vitro* whole-cell patch clamp experiments on L5 pyramidal neurons in the mouse prefrontal cortex (PFC) during extracellular electric stimulations of basal and apical afferents (**Fig. 4A**).

We recorded basally-induced baseline EPSPs for 5 minutes to establish initial synaptic responses. Next, we increased basal stimulation intensity to induce a single action potential and further adjusted apical stimulation intensity to provoke supra-threshold events that consisted of one, two, or three action potentials and prolonged somatic depolarization. After repeating these paired stimulation-induced supra-threshold events (PSSTs) 8 times, we again recorded basally-induced EPSPs for at least 30 minutes to measure long-term changes in EPSP amplitudes (**Fig. 4B**, for details see **Methods 7.1**). We conducted all recordings in physiological extracellular calcium concentrations under which LTP has been shown not to occur following basic STDP pairings (Inglebert et al., 2020).

Comparing basally-induced EPSPs before and after PSST, we found that some stimulation variants led to significantly increased EPSP amplitudes indicative of LTP (**Fig. 4C-D-E top**), while others resulted in no discernible change in EPSP amplitudes (**Fig. 4C-D-E bottom**).

To explain the observed variance in the EPSP amplitude changes we evaluated potential predictors of basal synaptic plasticity. We correlated the number of APs and the area under the curve of the somatic membrane depolarisation during PSSTs (PSST-AUC) to the change in EPSP amplitudes. We found a significant positive correlation between the membrane depolarization AUC and Δ EPSP ($R_{Spearman} = 0.8671$, $p = 0.0003$, **Fig. 4F**). In contrast, the correlation between the number of APs and Δ EPSP was $R_{Spearman} = 0.4286$, $p = 0.1645$ (**Fig. 4G**). This indicates that the total somatic depolarization that follows synaptic input is a better proxy to predict changes in synaptic strength than the number of APs following synaptic input. We note that the prolonged somatic depolarization resulting from dendritic plateau potentials can lead to burst firing (Larkum et al., 1999), indicating a dependency between the number of action potentials and the PSST-AUC. In this regard, we indeed find that the number of APs increases with the measured PSST-AUC (**Fig. 4H**), and that even on a single neuron basis, the change in the number of APs significantly depends on the PSST-AUC (**Fig. 4I**). Our recordings also contain data for apical synapses showing that changes in apical synaptic strength do not seem to follow the same plasticity rules found in basal synapses (for details see **Sec. 8.2** and **Supp. Fig. 8.2**).

In summary, we show that increased apical stimulation strength leads to prolonged somatic depolarization, which in turn results in increased numbers of APs, and is indicative of basal synaptic plasticity. These results, as well as previous literature, are consistent with our neuron model where apical inputs drive basal plasticity (Godenzini et al., 2022) and have a multiplicative effect on firing rate at the soma (Larkum et al., 2004).

3.6 Implementing hierarchical learning in multi-layer neuronal networks using calcium-dependent synaptic plasticity

After validating our pyramidal neuron model, we next explore whether the model demonstrates the capability of learning hierarchical neural representations (Yamins and DiCarlo, 2016; Khaligh-Razavi and Kriegeskorte, 2014b) as observed in multi-layer (deep) neuronal networks.

A fundamental requirement to successfully train deep neural networks is to compute neuron-

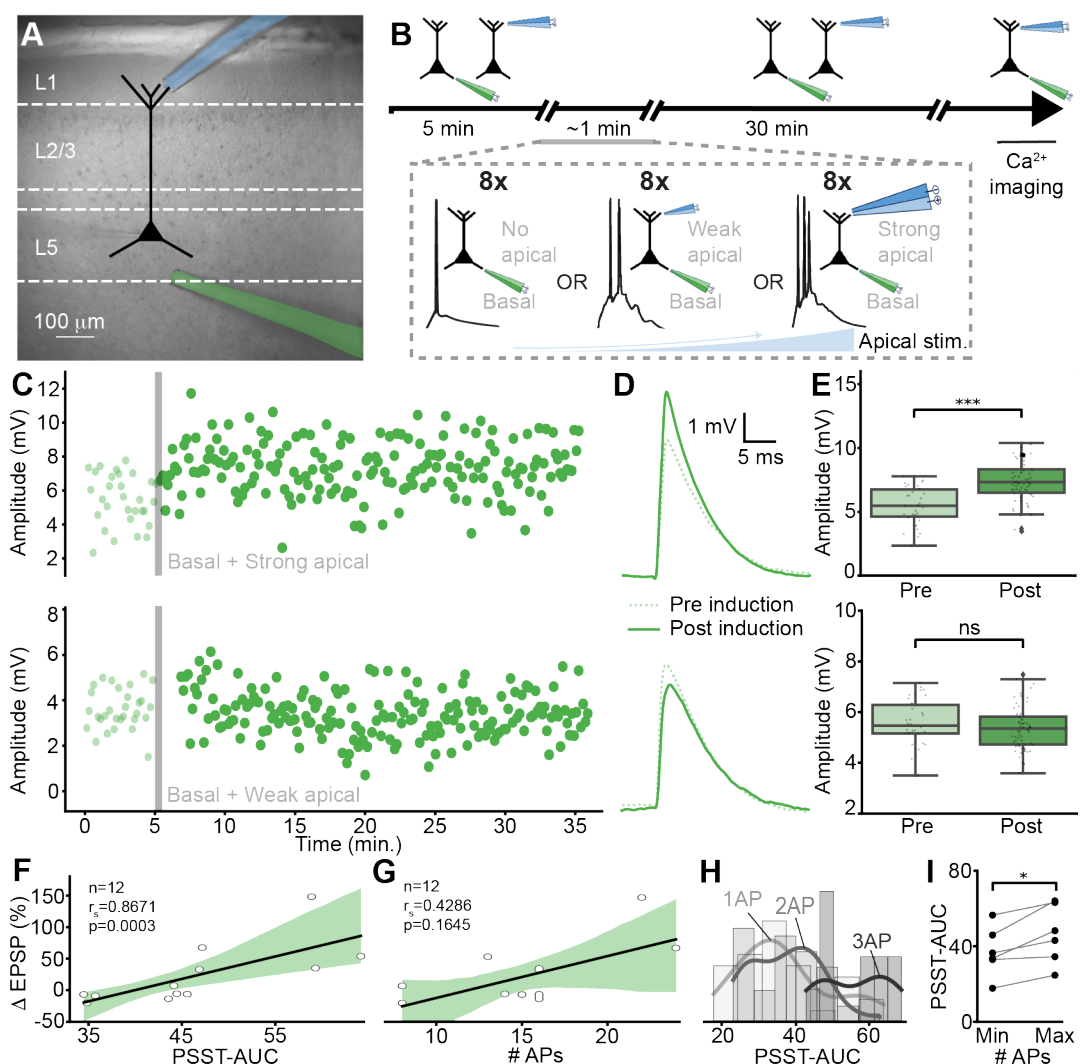


Figure 4: Apical inputs direct changes in synaptic strength in basal synapses. (A) Wide-field image of mouse PFC (L5 pyramidal neuron sketch superimposed) and placement of extracellular basal and apical stimulation electrodes. (B) Stimulation and recording protocol. (C–D–E) Example recordings of basal EPSP amplitudes before and after plasticity induction event with observed increase (top) and no change in synaptic strength (bottom). (C) EPSP amplitude evolution over time. (D) Mean EPSP pre and post-induction event. (E) Quantification of ΔEPSP (Student T-test, top, $p = 2.78e-06$, bottom, $p = 0.229$). (F–G) Linear correlation analysis between changes in basal EPSP amplitude and PSST-AUC and number of APs, respectively. (H) Histogram of the somatic membrane potential AUC of the plasticity induction event for 1, 2, and 3 APs. (I) Pairwise comparison of PSST-AUC for the minimum and maximum number of somatic APs (Wilcoxon signed-rank test, $p = 0.031$).

Framework	Test Error (%)		Hierarchical Clustering Metric							
	MNIST	F-MNIST	MNIST				F-MNIST			
			L0	L1	L2	L3	L0	L1	L2	L3
BP	1.83 ± 0.08	10.60 ± 0.34	0.75	1.44	4.02	10.16	2.03	2.10	4.11	8.32
EP	2.45 ± 0.15	12.77 ± 0.69	0.75	2.16	4.75	8.59	2.03	3.39	4.94	7.84
PC	2.29 ± 0.12	13.54 ± 0.28	0.75	1.92	6.21	14.12	2.03	2.45	4.86	9.66
DFC	2.01 ± 0.06	11.56 ± 0.46	0.75	1.19	2.24	4.41	2.03	3.28	3.32	4.52

Table 1: **Hierarchical learning with different network architectures.** Comparison of MNIST and Fashion-MNIST testing error ($\% \pm \text{S.D.}$) after 40 epoch training for a range of learning algorithms, namely Equilibrium Propagation (EP), Predictive Coding (PC), and Deep Feedback Control (DFC), compared to the Backpropagation (BP) algorithm. Neural representation separability measurement in input and hidden layers, with the input as layer 0 (L0).

specific, top-down teaching signals that individual neurons can use to update their synapses (Richards et al., 2019; Marblestone et al., 2016). While recent experiments support the presence of teaching signals (Francioni et al., 2023), the explicit neural circuitry and underlying algorithms that compute and implement teaching signals remain an open area of research. Various theoretical architectures and frameworks have been proposed to potentially explain the structure of cortical feedback signals (Rao and Ballard, 1999; Scellier and Bengio, 2017; Whittington and Bogacz, 2017; Sacramento et al., 2018; Meulemans et al., 2021; Payeur et al., 2021; Laborieux and Zenke, 2022; Meulemans et al., 2022a; Greedy et al., 2022; Meulemans et al., 2022b; Millidge et al., 2022; Laborieux and Zenke, 2023; Aceituno et al., 2023; Rosenbaum, 2022), which we evaluate to demonstrate that our pyramidal neuron model can integrate bottom-up basal inputs and top-down feedback in deep hierarchical networks.

Within these existing frameworks, we consider those that are compatible with target learning, where the teaching signal, here apical feedback, induces a change in somatic activity that drives individual neurons toward their target activities. Using this requirement as a selection criterion we adopted three main frameworks that fulfill this requirement: (1) Equilibrium Propagation (Scellier and Bengio, 2017), (2) a variant of Predictive Coding (Rao and Ballard, 1999) that allows training of deep networks in a supervised setting (Whittington and Bogacz, 2017), and (3) Deep Feedback Control (Meulemans et al., 2021).

Given the computational complexity of simulating continuous time models with spiking dynamics and computing precise feedback values, we follow previous approaches (Rao and Ballard, 1999; Scellier and Bengio, 2017; Whittington and Bogacz, 2017; Sacramento et al., 2018; Meulemans et al., 2021; Payeur et al., 2021; Laborieux and Zenke, 2022; Meulemans et al., 2022a; Greedy et al., 2022; Meulemans et al., 2022b; Millidge et al., 2022; Laborieux and Zenke, 2023; Aceituno et al., 2023; Rosenbaum, 2022) and convert our spiking neuron model to a rate based formulation (see **Methods 7.2** and **Supp. Fig. 8**). This allows us to adopt the three above-mentioned network architectures with only minor modifications (see **Discussion** and **Methods 7.4** for an explanation of the adaptation).

To provide a direct assessment of successful network training that can be equally applied to all architectures, we focus on supervised learning tasks. We train our architectures on MNIST and Fashion-MNIST (LeCun et al., 1998; Xiao et al., 2017), two standard machine learning benchmarks that require the emergence of hierarchical representations to achieve state-of-the-art classification

performances (error rates of 1.83% and 10.6%, respectively). We find that all the proposed architectures achieve error rates that are close to those achieved by backpropagation of error (see **Table 1**), suggesting that our single neuron model is indeed capable of hierarchical learning when integrated within the aforementioned target-learning architectures. To further verify that learning promotes the emergence of hierarchies, we also evaluate whether the representations of sensory inputs become more aligned with their output across the hierarchy. We therefore measure the separability between classes of the neural representations across the hierarchy (see **Methods 7.5**). As expected, we find that for all the architectures the neural representations become more distinct, that is, more informative of the respective output, in higher layers (see **Table 1** and **Supp. Fig. 9**).

4 Discussion

Hierarchical learning in the mammalian neocortex relies on the integration of feedforward and feedback signals that arrive at different locations within a pyramidal neuron. To investigate how their integration enables hierarchical learning, we built a L5 pyramidal neuron model grounded on a wide range of experimental findings such as calcium-based synaptic plasticity, bAPs, plateau potentials, bursting and apical-somatic coupling. Using our neuron model, we then predicted how plasticity at basal synapses is organized, and validated this prediction experimentally. At the single neuron level, our modeling and *in vitro* data provide new evidence supporting target learning (Lee et al., 2014; Meulemans et al., 2020; Song et al., 2024). In this paradigm, individual neurons receive top-down apical input that imposes a target activity, and drives basal synaptic plasticity, ensuring that neurons maintain this activity even without feedback. At the network level, we combine our neuron model with various network architectures that support the top-down propagation of apical feedback, allowing a straightforward training of deep artificial networks that form hierarchical representations. These findings provide some first evidence that cortical hierarchies might form by utilizing target learning, instead of the classical error backpropagation method used in deep learning.

The core difference between error backpropagation and target learning resides in the treatment of somatic activity and learning signals: While backpropagation and biological approximations thereof (Sacramento et al., 2018; Payeur et al., 2021) use separate pathways for feedforward sensory information and the errors that drive plasticity, in target learning these signals are combined into a single input that simultaneously affects both the somatic activity and plasticity (Rao and Ballard, 1999; Scellier and Bengio, 2017; Whittington and Bogacz, 2017; Meulemans et al., 2021). Our *in vitro* experiments show that in pyramidal neurons, the integration of learning signals and sensory information is implemented through plateau potentials, which are necessary for learning and also have a significant effect on somatic activity (**Fig. 4**). This tight coupling of feedback-driven somatic activity and plasticity is also consistent with spike-based plasticity models such as STDP, which can be used for training neural networks using target learning (Aceituno et al., 2023; Bengio et al., 2017), but goes beyond most plasticity models that solely consider the number or the timing of post-synaptic APs (Feldman, 2012; Caporale and Dan, 2008; Sjöström et al., 2010; Pfister and Gerstner, 2006).

We note that even though our model and experiments argue in favor of target learning, we cannot fully exclude the possibility that the cortex approximates backpropagation learning. Given the complexity of cortical microcircuits, constructing a network architecture around our neuron model that cancels out the effect of the apical input on somatic activity is possible. For example, a circuit in which each pyramidal neuron gets input from an individually tuned inhibitory cell can compensate for the bursting generated by apical inputs, making neural activity independent of the learning signal (Sacramento et al., 2018). This would, however, require similar numbers of excitatory and inhibitory

neurons within a specific circuit design in the cortex. Alternatively, unidirectional synaptic filtering could prevent burst spikes triggered by apical inputs from propagating upwards in the hierarchy (Payeur et al., 2021). However, this has not yet been observed and would conflict with reports that bursts arriving at basal dendrites affect the activity of postsynaptic neurons (Markram, 1997; Lisman, 1997; Malinow et al., 1994). A third alternative would be to utilize small feedback errors that only minimally affect somatic activity (Whittington and Bogacz, 2017). However, previous studies as well as our single neuron data suggest that the effect of apical feedback on somatic activity is strong and multiplicative (Larkum et al., 2004). In addition, how small error signals could efficiently back-propagate in noisy biological environments is currently unclear (Meulemans et al., 2022a). More generally, any implementation of backpropagation-like learning would require (or result in) symmetric forward and backward weights (Amit, 2019; Liao et al., 2016; Grossberg, 1987; Lillicrap et al., 2016). In the cortex, this would require aligned synaptic learning for both bottom-up and top-down signaling pathways (Akrout et al., 2019; Amit, 2019). However, our data suggests a difference in apical and basal synaptic plasticity (see **Fig. 4**), inconsistent with the idea of weight symmetry.

The next question is then to identify and understand the circuits and underlying computations that determine apical feedback and its plasticity. Using our stimulation protocol (**Fig. 4B**) we find differences in basal versus apical synaptic plasticity, which the unspecific nature of our apical stimulation could explain. As we stimulate apical dendrites using extracellular electrodes, we most likely jointly activated axons from the contralateral prefrontal cortex (cPFC) as well as thalamic nuclei, specifically the mediodorsal (MD) and ventromedial (VM) thalamus (Anastasiades and Carter, 2021). Projections from MD thalamus not only activate inhibitory interneurons within local disinhibitory circuits but also include excitatory synapses on apical dendrites (Williams and Holtmaat, 2019). As different neuron types likely have different synaptic plasticity rules, this could explain the observed differences in apical and basal synaptic plasticity. From a functional perspective, a recent study has shown that, the neuronal response to apical inputs encoding reward decreases during learning, while the response to associated context increases (Schoenfeld et al., 2022). Future work should attempt to disentangle the contributions of different afferent projections to elicit apical input and drive plasticity, for example using optogenetic methods.

From a computational perspective, the main limitation of our work is the computational complexity when training continuous-time, dynamic network models for target learning at scale. Target learning has gained some attention in machine learning due to its potential advantages over back-propagation of error in problems involving continual learning and generalization (Lässig et al., 2023; Song et al., 2024; Fairbank et al., 2022). However, biological models using target learning require a simulation of network dynamics in continuous time, where feedforward and feedback passes are iterated hundreds of times for every data sample (Meulemans et al., 2021; Rao and Ballard, 1999; Scellier and Bengio, 2017), rendering the training process hundreds of times slower than in conventional learning frameworks. Furthermore, most modern deep networks use convolutional layers to increase data efficiency and decrease training time, which do not yet exist for biological target-learning architectures. In short, to reach state-of-the-art performances in more competitive datasets such as CIFAR or ImageNet, target learning network architectures will require further advances.

To conclude, our data and simulations on cortical learning connect several scales of neural learning and provide preliminary evidence that cortical networks may learn differently than their artificial counterparts. Future theoretical and experimental studies can leverage our neuron model to investigate how apical projections from different areas drive learning and computation. Moreover, from a computational perspective, recognizing that brains learn distinctively from existing machine learning models could inspire the development of novel and improved deep learning systems.

5 Author contributions

P.V.A. conceptualized the project and the modelling experiments. P.V.A. and S.d.H. developed the single neuron model. P.V.A. performed the mathematical descriptions of the model. S.d.H. implemented the single neuron model and deep learning models, and performed the simulations. R.L. conceptualized and performed the electrophysiological experiments. R.L. provided biology insights about the project on both theoretical and experimental neuroscience. B.F.G. supervised the project. P.V.A., S.d.H., R.L., and B.F.G. wrote the paper.

6 Acknowledgements

This work was supported by the Swiss National Science Foundation (B.F.G. CRSII5-173721 and 315230 189251), ETH project funding (B.F.G. ETH-20 19-01), the Human Frontiers Science Program (RGY0072/2019) and funding from the Swiss Data Science Center (B.F.G, C17-18). P.V.A. was supported by an ETH Zurich Postdoc fellowship.

References

- Aceituno, P. V., Farinha, M. T., Loidl, R., and Grewe, B. F. (2023). Learning Cortical Hierarchies with Temporal Hebbian Updates. *bioRxiv* doi:10.1101/2023.01.02.522459
- Akrout, M., Wilson, C., Humphreys, P., Lillicrap, T., and Tweed, D. B. (2019). Deep learning without weight transport. *Advances in neural information processing systems* 32
- Amit, Y. (2019). Deep learning with asymmetric connections and hebbian updates. *Frontiers in computational neuroscience* 13, 18
- Anastasiades, P. G. and Carter, A. G. (2021). Circuit organization of the rodent medial prefrontal cortex. *Trends in neurosciences* 44, 550–563
- Artola, A. and Singer, W. (1987). Long-term potentiation and nmda receptors in rat visual cortex. *Nature* 330, 649–652
- Bannister, A. P. (2005). Inter-and intra-laminar connections of pyramidal cells in the neocortex. *Neuroscience research* 53, 95–103
- Bear, M. F., Press, W. A., and Connors, B. W. (1992). Long-term potentiation in slices of kitten visual cortex and the effects of nmda receptor blockade. *Journal of Neurophysiology* 67, 841–851
- Bengio, Y., Mesnard, T., Fischer, A., Zhang, S., and Wu, Y. (2017). STDP-Compatible Approximation of Backpropagation in an Energy-Based Model. *Neural Computation* 29, 555–577. doi: 10.1162/NECO_a_00934
- Caporale, N. and Dan, Y. (2008). Spike timing-dependent plasticity: a hebbian learning rule. *Annu. Rev. Neurosci.* 31, 25–46
- Chindemi, G., Abdellah, M., Amsalem, O., Benavides-Piccione, R., Delattre, V., Doron, M., et al. (2022). A calcium-based plasticity model for predicting long-term potentiation and depression in the neocortex. *Nature Communications* 13, 3038. doi:10.1038/s41467-022-30214-w

- Evans, R. and Blackwell, K. (2015). Calcium: Amplitude, Duration, or Location? *The Biological bulletin* 228, 75–83
- Fairbank, M., Samothrakis, S., and Citi, L. (2022). Deep learning in target space. *Journal of Machine Learning Research* 23, 1–46
- Feldman, D. E. (2012). The Spike-Timing Dependence of Plasticity. *Neuron* 75, 556–571. doi: 10.1016/j.neuron.2012.08.001
- Fisek, M., Herrmann, D., Egea-Weiss, A., Cloves, M., Bauer, L., Lee, T.-Y., et al. (2023). Cortico-cortical feedback engages active dendrites in visual cortex 617, 769–776. doi:10.1038/s41586-023-06007-6
- Francioni, V., Tang, V. D., Brown, N. J., Toloza, E. H., and Harnett, M. (2023). Vectorized instructive signals in cortical dendrites during a brain-computer interface task. *bioRxiv*
- Godenzini, L., Shai, A. S., and Palmer, L. M. (2022). Dendritic compartmentalization of learning-related plasticity. *Eneuro* 9
- Graupner, M. and Brunel, N. (2012). Calcium-based plasticity model explains sensitivity of synaptic changes to spike pattern, rate, and dendritic location. *Proceedings of the National Academy of Sciences* 109, 3991–3996. doi:10.1073/pnas.1109359109
- Greedy, W., Zhu, H. W., Pemberton, J., Mellor, J., and Ponte Costa, R. (2022). Single-phase deep learning in cortico-cortical networks. *Advances in Neural Information Processing Systems* 35, 24213–24225
- Grewen, B., Bonnan, A., and Frick, A. (2010). Back-propagation of physiological action potential output in dendrites of slender-tufted L5A pyramidal neurons. *Frontiers in Cellular Neuroscience* 4
- Grossberg, S. (1987). Competitive learning: From interactive activation to adaptive resonance. *Cognitive science* 11, 23–63
- Gulledge, A. T. and Stuart, G. J. (2003). Action Potential Initiation and Propagation in Layer 5 Pyramidal Neurons of the Rat Prefrontal Cortex: Absence of Dopamine Modulation. *The Journal of Neuroscience* 23, 11363–11372. doi:10.1523/JNEUROSCI.23-36-11363.2003
- Honnuraiah, S. and Narayanan, R. (2013). A calcium-dependent plasticity rule for HCN channels maintains activity homeostasis and stable synaptic learning. *PloS One* 8. doi: 10.1371/journal.pone.0055590
- Inglebert, Y., Aljadeff, J., Brunel, N., and Debanne, D. (2020). Synaptic plasticity rules with physiological calcium levels. *Proceedings of the National Academy of Sciences of the United States of America* 117, 33639–33648. doi:10.1073/pnas.2013663117
- Kasper, E. M., Larkman, A. U., Lübke, J., and Blakemore, C. (1994). Pyramidal neurons in layer 5 of the rat visual cortex. I. Correlation among cell morphology, intrinsic electrophysiological properties, and axon targets. *The Journal of Comparative Neurology* 339, 459–474. doi: 10.1002/cne.903390402
- Khaligh-Razavi, S.-M. and Kriegeskorte, N. (2014a). Deep supervised, but not unsupervised, models may explain it cortical representation. *PLoS computational biology* 10, e1003915

- Khaligh-Razavi, S.-M. and Kriegeskorte, N. (2014b). Deep Supervised, but Not Unsupervised, Models May Explain IT Cortical Representation. *PLOS Computational Biology* 10. doi: 10.1371/journal.pcbi.1003915
- Laborieux, A. and Zenke, F. (2022). Holomorphic equilibrium propagation computes exact gradients through finite size oscillations. *Advances in Neural Information Processing Systems* 35, 12950–12963
- Laborieux, A. and Zenke, F. (2023). Improving equilibrium propagation without weight symmetry through jacobian homeostasis. *arXiv preprint arXiv:2309.02214*
- Larkum, M., Zhu, J., and BJ, S. (2001). Dendritic mechanisms underlying the coupling of the dendritic with the axonal action potential initiation zone of adult rat layer 5 pyramidal neurons. *The Journal of physiology* 533, 447–66. doi:10.1111/j.1469-7793.2001.0447a.x
- Larkum, M. E., Senn, W., and Lüscher, H.-R. (2004). Top-down dendritic input increases the gain of layer 5 pyramidal neurons. *Cerebral Cortex (New York, N.Y.: 1991)* 14, 1059–1070. doi:10.1093/cercor/bhh065
- Larkum, M. E., Zhu, J. J., and Sakmann, B. (1999). A new cellular mechanism for coupling inputs arriving at different cortical layers. *Nature* 398, 338–341. doi:10.1038/18686
- Lässig, F., Aceituno, P. V., Sorbaro, M., and Grewe, B. F. (2023). Bio-inspired, task-free continual learning through activity regularization. *Biological Cybernetics* 117, 345–361
- LeCun, Y., Bottou, L., Bengio, Y., and Haffner, P. (1998). Gradient-based learning applied to document recognition. *Proceedings of the IEEE* 86, 2278–2324
- Lee, D.-H., Zhang, S., Fischer, A., and Bengio, Y. (2014). Difference Target Propagation. *arXiv* doi:10.48550/arXiv.1412.7525
- Liao, Q., Leibo, J., and Poggio, T. (2016). How important is weight symmetry in backpropagation? In *Proceedings of the AAAI Conference on Artificial Intelligence*. vol. 30
- Lillicrap, T. P., Cownden, D., Tweed, D. B., and Akerman, C. J. (2016). Random synaptic feedback weights support error backpropagation for deep learning. *Nature Communications* 7, 13276. doi: 10.1038/ncomms13276
- Lisman, J. (1989). A mechanism for the Hebb and the anti-Hebb processes underlying learning and memory. *Proceedings of the National Academy of Sciences of the United States of America* 86, 9574–9578. doi:10.1073/pnas.86.23.9574
- Lisman, J. E. (1997). Bursts as a unit of neural information: making unreliable synapses reliable. *Trends in neurosciences* 20, 38–43
- Majewska, A., Brown, E., Ross, J., and Yuste, R. (2000). Mechanisms of Calcium Decay Kinetics in Hippocampal Spines: Role of Spine Calcium Pumps and Calcium Diffusion through the Spine Neck in Biochemical Compartmentalization. *The Journal of Neuroscience* 20, 1722–1734. doi: 10.1523/JNEUROSCI.20-05-01722.2000
- Malinow, R., Otmakhov, N., Blum, K. I., and Lisman, J. (1994). Visualizing hippocampal synaptic function by optical detection of Ca^{2+} entry through the $\text{n-methyl-d-aspartate}$ channel. *Proceedings of the National Academy of Sciences* 91, 8170–8174

- Marblestone, A. H., Wayne, G., and Kording, K. P. (2016). Toward an integration of deep learning and neuroscience. *Frontiers in computational neuroscience* 10, 94
- Markram, H. (1997). A network of tufted layer 5 pyramidal neurons. *Cerebral cortex (New York, NY: 1991)* 7, 523–533
- Markram, H., Lübke, J., Frotscher, M., and Sakmann, B. (1997). Regulation of synaptic efficacy by coincidence of postsynaptic APs and EPSPs. *Science (New York, N.Y.)* 275, 213–215. doi: 10.1126/science.275.5297.213
- McRory, J. E., Santi, C. M., Hamming, K. S. C., Mezeyova, J., Sutton, K. G., Baillie, D. L., et al. (2001). Molecular and Functional Characterization of a Family of Rat Brain T-type Calcium Channels. *Journal of Biological Chemistry* 276, 3999–4011. doi:10.1074/jbc.M008215200
- Meulemans, A., Carzaniga, F. S., Suykens, J. A., Sacramento, J., and Grewe, B. F. (2020). A theoretical framework for target propagation. In *Proceedings of the 34th International Conference on Neural Information Processing Systems* (Red Hook, NY, USA: Curran Associates Inc.), NIPS’20, 20024–20036
- Meulemans, A., Farinha, M. T., Cervera, M. R., Sacramento, J., and Grewe, B. F. (2022a). Minimizing control for credit assignment with strong feedback. In *International Conference on Machine Learning* (PMLR), 15458–15483
- Meulemans, A., Tristany Farinha, M., Garcia Ordóñez, J., Vilimelis Aceituno, P., Sacramento, J. a., and Grewe, B. F. (2021). Credit assignment in neural networks through deep feedback control. In *Advances in Neural Information Processing Systems* (Curran Associates, Inc.), vol. 34, 4674–4687
- Meulemans, A., Zucchetti, N., Kobayashi, S., Von Oswald, J., and Sacramento, J. (2022b). The least-control principle for local learning at equilibrium. *Advances in Neural Information Processing Systems* 35, 33603–33617
- Millidge, B., Tschantz, A., and Buckley, C. L. (2022). Predictive coding approximates backprop along arbitrary computation graphs. *Neural Computation* 34, 1329–1368
- Nevian, T. and Sakmann, B. (2006). Spine Ca²⁺ Signaling in Spike-Timing-Dependent Plasticity. *The Journal of Neuroscience* 26, 11001–11013. doi:10.1523/JNEUROSCI.1749-06.2006
- Payeur, A., Guerguiev, J., Zenke, F., Richards, B. A., and Naud, R. (2021). Burst-dependent synaptic plasticity can coordinate learning in hierarchical circuits. *Nature Neuroscience* 24, 1010–1019. doi:10.1038/s41593-021-00857-x
- Petreanu, L., Mao, T., Sternson, S. M., and Svoboda, K. (2009). The subcellular organization of neocortical excitatory connections. *Nature* 457, 1142–1145
- Pfister, J.-P. and Gerstner, W. (2006). Triplets of spikes in a model of spike timing-dependent plasticity. *Journal of Neuroscience* 26, 9673–9682
- Rao, R. P. N. and Ballard, D. H. (1999). Predictive coding in the visual cortex: a functional interpretation of some extra-classical receptive-field effects. *Nature Neuroscience* 2, 79–87. doi: 10.1038/4580
- Richards, B. A., Lillicrap, T. P., Beaudoin, P., Bengio, Y., Bogacz, R., Christensen, A., et al. (2019). A deep learning framework for neuroscience. *Nature neuroscience* 22, 1761–1770

- Rosenbaum, R. (2022). On the relationship between predictive coding and backpropagation. *PLOS ONE* 17, 1–27. doi:10.1371/journal.pone.0266102
- Sacramento, J., Ponte Costa, R., Bengio, Y., and Senn, W. (2018). Dendritic cortical microcircuits approximate the backpropagation algorithm. In *Advances in Neural Information Processing Systems* (Curran Associates, Inc.), vol. 31, 8735–8746
- Scellier, B. and Bengio, Y. (2017). Equilibrium propagation: Bridging the gap between energy-based models and backpropagation. *Frontiers in computational neuroscience* 11, 24
- Schoenfeld, G., Kollmorgen, S., Lewis, C., Bethge, P., Reuss, A. M., Aguzzi, A., et al. (2022). Dendritic integration of sensory and reward information facilitates learning. *bioRxiv* doi: 10.1101/2021.12.28.474360
- Sjöström, J., Gerstner, W., et al. (2010). Spike-timing dependent plasticity. *Spike-timing dependent plasticity* 35, 0–0
- Sjöström, P. J., Turrigiano, G. G., and Nelson, S. B. (2003). Neocortical ltd via coincident activation of presynaptic nmda and cannabinoid receptors. *Neuron* 39, 641–654
- Slutsky, I., Sadeghpour, S., Li, B., and Liu, G. (2004). Enhancement of Synaptic Plasticity through Chronically Reduced Ca²⁺ Flux during Uncorrelated Activity. *Neuron* 44, 835–849. doi:10.1016/j.neuron.2004.11.013
- Song, Y., Millidge, B., Salvatori, T., Lukasiewicz, T., Xu, Z., and Bogacz, R. (2024). Inferring neural activity before plasticity as a foundation for learning beyond backpropagation. *Nature Neuroscience* , 1–11
- Stuart, G., Schiller, J., and Sakmann, B. (1997). Action potential initiation and propagation in rat neocortical pyramidal neurons. *The Journal of Physiology* 505, 617–632
- van der Maaten, L. and Hinton, G. (2008). Viualizing data using t-sne. *Journal of Machine Learning Research* 9, 2579–2605
- Whittington, J. C. R. and Bogacz, R. (2017). An Approximation of the Error Backpropagation Algorithm in a Predictive Coding Network with Local Hebbian Synaptic Plasticity. *Neural Computation* 29, 1229–1262. doi:10.1162/NECO_a_00949
- Williams, L. E. and Holtmaat, A. (2019). Higher-Order Thalamocortical Inputs Gate Synaptic Long-Term Potentiation via Disinhibition. *Neuron* 101, 91–102. doi:10.1016/j.neuron.2018.10.049
- [Dataset] Xiao, H., Rasul, K., and Vollgraf, R. (2017). Fashion-mnist: a novel image dataset for benchmarking machine learning algorithms
- Yamins, D. L. K. and DiCarlo, J. J. (2016). Using goal-driven deep learning models to understand sensory cortex. *Nature neuroscience* 19, 356–365
- Yang, S. N., Tang, Y. G., and Zucker, R. S. (1999). Selective induction of LTP and LTD by postsynaptic [Ca²⁺]i elevation. *Journal of Neurophysiology* 81, 781–787. doi:10.1152/jn.1999.81.2.781

7 Methods

7.1 Electrophysiology

Male B6/J-Crl1 mice of strain C57BL/6J (orig. Charles River) were bred and maintained at our in-house facility. Animals were kept in their home cages under normal day/night conditions (light: 7am – 7pm). Mouse experiments were approved by the institutional animal care and use committee of the University of Zurich. All experiments were conducted with the approval of the Cantonal Veterinary Office Zurich.

Mice (11-13 weeks old) were deeply anesthetized using Isoflurane and decapitated. The brains were dissected from the skull and submerged in ice-cold high-sucrose artificial cerebrospinal fluid (ACSF) during acute slice preparation. High sucrose ACSF containing (in mM): 75 Sucrose, 10 Glucose, 80 NaCl, 26 NaHCO₃, 7 MgSO₄, 2.5 KCl, 1 NaH₂PO₄, 0.5 CaCl₂, fumigated with oxycarbon (95% O₂, 5% CO₂). Coronal slices (300 µm) were drawn from PFC (+1.4 to +2.6 from bregma) using a VT1200 S vibratome (Leica) and incubated for 30 minutes in oxygenated holding ACSF at 36°C. Holding ACSF containing (in mM): 15 Glucose, 120 NaCl, 26 NaHCO₃, 0.9 MgSO₄, 2.5 KCl, 1.25 NaH₂PO₄, 1.3 CaCl₂, fumigated with oxycarbon (95% O₂, 5% CO₂). Slices rested for at least 45 minutes in holding ACSF at room temperature prior to electrophysiological recordings.

Neurons were visualized with differential interference contrast (DIC) using an Olympus BX61 WI microscope with an Olympus 60x water immersion objective and a CellCam Kikker MT100 (Cairn) DCIM camera. L5 pyramidal neurons (PN) in the PFC were identified based on morphology and distance to the pia and patched with glass pipettes with resistances of 4.8-6.4 MΩ filled with intracellular solution containing (in mM): 10 HEPES, 20 KCl, 117 K-gluconate, 4 Mg-ATP, 0.3 GTP, 10 Na-P-creatine. In neurons for morphology reconstruction, the intracellular solution also contained 0.2% Biocytin. For neurons patched for Ca²⁺ imaging, the intracellular solution also contained 200 µM Oregon Green™ 488 BAPTA-5N. Whole-cell, somatic patch-clamp recordings were acquired in current-clamp mode using an Axon MultiClamp 700A amplifier and digitized using an Axon DigiData 1550 B digital converter. Data was sampled at 50 kHz and filtered at 3 kHz. Typical resting membrane potentials were between -64mV and -72mV, and access resistance ranged from 15 MΩ to 25 MΩ. Recordings in which neurons depolarized > 10% from resting potential or access resistance changed > 15% from initial value were discarded. Bridge potentials were compensated, and liquid-junction potentials were not corrected for. Depolarizing and hyperpolarizing currents were injected to characterize neurons further. Only neurons showing L5 PN-typical *I_h*-currents were considered. Theta-barrel glass-pipettes with openings of 30 µm were placed at 50 µm – 80 µm from the patched neuron to stimulate afferents targeting basal dendrites as well as in cortical layer 1 to stimulate apical afferents with synapses onto apical tuft dendrites.

After stabilization of resting membrane potential, apical and basal stimulation strength was adjusted to elicit EPSPs with amplitudes in the range of 2-3 mV. This usually required 100 µs voltage pulses in the range of -1 to -3 V followed by immediate 100 µs voltage pulses of +1 to +3 V for basal stimulations. Apical stimulation had the same shape but ranged from -6 to -8 V and +6 to +8 V, respectively. Next, the required strength of basal stimulations to induce a single action potential was determined. For this, tripling basal stimulation amplitudes and stimulating 3 times at 100 Hz was usually sufficient. If extracellular electrical stimulation was not sufficient to trigger action potentials, additional current was injected into the soma via the patch pipette until an AP was induced. Finally, apical stimulation strength was increased until multiple action potentials or plateau potentials were induced.

After all required stimulation amplitudes were set, baseline EPSP amplitudes were recorded for 5 minutes with alternating basal and apical stimulations every 5 seconds followed by 8 combined,

strong basal and apical stimulations with a 10 second interval, each eliciting a plasticity induction event. Next, EPSPs were recorded for at least 30 minutes (same as baseline recordings).

Analysis of electrophysiology traces was performed using individual Python scripts and the pyabf library. The correlation analyses were performed with the seaborn library (regplot) and the statistical analysis with the scipy library (spearmanr).

Analysis of PSST-AUC with different numbers of action potentials (**Fig. 4K**) was performed on a subset of neurons in which PSSTs occurred with different amounts of APs (1vs2, 1vs3, or 2vs3). PSST-AUCs were averaged for events with min. and max. number of APs respectively and plotted as 2 data points per cell.

In the case of cell morphology reconstruction (only performed in 8 of 12 neurons), slices were kept in 4% PFA for 24-32 hours and stained overnight with Streptavidin, Alexa Fluor 350 conjugate (invitrogen) and mounted on commercially available microscopy slides.

Calcium imaging was performed in a subset of neurons ($n = 7$ neurons, 4 mice) after post-induction EPSP recordings where completed by imaging pipette-filled OGB5-N using a Lumencor SPECTRA Light Engine (GFP/FITC 475/28 nm) for excitation and a ORCA-Lightning Digital CMOS camera (C14120-20P, Hamamatsu) for image acquisition at 50 Hz. Imaging data was pre-processed (background-subtraction, bleaching correction) using Fiji/ImageJ2. Extracted fluorescence traces were further processed and analysed using individual Python scripts. A correlation analysis between somatic calcium recordings (derived as $\Delta F/F$ AUC) and somatic membrane potential AUC showed a significant correlation ($R_{Spearman} = 0.8303$, $p = 0.0029$) and was used to infer calcium levels during the actual plasticity induction events using linear regression.

Group data are expressed as mean \pm s.e.m. unless otherwise stated. Statistical significance was calculated using paired or unpaired t-tests as well as Spearman correlation.

7.2 Derivation of the rate-based neuron model

The inputs that arrive at the soma and the inputs that arrive at the apical dendrites are assumed to follow a Poisson distribution with a relatively low firing rate, in order to ensure that consecutive presynaptic spikes or feedback spikes are temporally separated with high probability, allowing us to consider spikes and bursts as independent events.

We divide the somatic output into bursts and single spikes. The number of events where somatic presynaptic input drove the soma over the threshold θ_{soma} is represented by N . The events will sometimes generate a burst N_{burst} and sometimes a single spike N_{spike} , thus $N = N_{\text{burst}} + N_{\text{spike}}$. A burst is generated only if feedback input arrives at the apical dendrites within a short time interval ΔT after a somatic postsynaptic spike. Using the aforementioned assumption of low firing rates for apical and somatic inputs, which implies that somatic spikes cannot arrive very close in time, coincidence of basal and apical inputs are independent events. We can thus calculate the expected number of bursts and single APs

$$N_{\text{burst}} = \frac{\Delta T}{T} r_{\text{apical}} N, \quad N_{\text{spike}} = (1 - \frac{\Delta T}{T} r_{\text{apical}}) N \quad (6)$$

where T represents the total time of the simulation, and r_{apical} is the rate of feedback input. Intuitively, the number of bursts is simply the fraction of time at which the apical input can generate a burst times the probability of receiving suprathreshold somatic activity.

Lastly, the firing rate of the postsynaptic neuron increases when burst firing occurs. Therefore, considering the firing rate as the number of spikes, the firing rate can be expressed as,

$$r_{\text{post}} = N_{\text{spike}} + \bar{m}N_{\text{burst}} = N \left(\bar{m} + \frac{\Delta T}{T} r_{\text{apical}}(1 - \bar{m}) \right). \quad (7)$$

where $\bar{m} > 1$ is the expected number of spikes per burst. As denoted here, the expected firing rate of the neuron grows monotonically with the amount of apical feedback.

We can now derive plasticity from the calcium model, understanding that a plateau potential generates LTP, and a burst and a single spike without the corresponding apical input generates LTD when there is a presynaptic spike

$$\Delta w = [\Delta_{\text{burst}} w N_{\text{burst}} - \Delta_{\text{spike}} w N_{\text{spike}}] \frac{N_{\text{pre}}}{T} \quad (8)$$

where $\Delta_{\text{burst}} w > 0$ and $\Delta_{\text{spike}} w > 0$ denote the synaptic change per burst or spike, respectively, and N_{pre} correspond to the number of presynaptic spikes. Substituting Eq. 6 into Eq. 8 produces,

$$\Delta w = \left(\frac{\Delta T}{T} N \frac{N_{\text{pre}}}{T} \right) (r_{\text{apical}}(\Delta_{\text{burst}} w + \Delta_{\text{spike}} w) - \frac{T}{\Delta T} \Delta_{\text{spike}} w). \quad (9)$$

Now there exist a r_{apical}^* such that $\Delta w = 0$, which corresponds to

$$r_{\text{apical}}^* = \frac{\frac{T}{\Delta T} \Delta_{\text{spike}} w}{\Delta_{\text{burst}} w + \Delta_{\text{spike}} w} \quad (10)$$

To make the aforementioned quantities amenable to standard plasticity models, we can note that the number of events of the neuron is a function of its presynaptic inputs, $N = \tilde{\phi} \left(\sum_{i \in \text{pre}} w_i r_i \right)$, giving us the simplified equation

$$\dot{r}_{\text{post}}(t) = -r_{\text{post}}(t) + \tilde{\phi} \left(\sum_{i \in \text{pre}} w_i r_i(t) \right) \left(\bar{m} + \frac{\Delta T}{T} r_{\text{apical}}(t)(1 - \bar{m}) \right) \quad (11)$$

$$= -r_{\text{post}}(t) + \tilde{\phi} \left(\sum_{i \in \text{pre}} w_i r_i(t) \right) (\bar{m} + \alpha r_{\text{apical}}(t)). \quad (12)$$

where $\tilde{\phi}$ is the response function of the neuron giving the number of suprathreshold events as a function of the input rates, and α is a scaling parameter that we will consider a unit for simplicity. To simplify the model further, we will consider a scaled response function $\phi(\cdot)$ for which the apical input is r_{apical}^* , which yields

$$\dot{r}_{\text{post}}(t) = -r_{\text{post}}(t) + \phi(z(t)) a(t), \quad (13)$$

where $a(t)$ is the apical input rescaled so that the default apical input $a^* = 1$, and $z(t) = \sum_{i \in \text{pre}} w_i r_i(t)$ is the overall basal stimulation at the neuron from all the presynaptic neurons.

We can use a similar logic to derive a simplified equation for the plasticity, where the firing depends on

$$\Delta w \propto \int r_{\text{pre}}(t) \phi(z(t)) (a(t) - a^*) dt \quad (14)$$

to simplify the computations, or if the network spends enough time at equilibrium, the equation for the plasticity can then be simplified to

$$\Delta w \propto r_{\text{pre}} \phi \left(\sum_{i \in \text{pre}} w_i r_i \right) (a - a^*) \quad (15)$$

where the lack of temporal dimension refers to the rates at equilibrium.

7.3 Proof of convergence in target-based learning paradigms

In this section, we derive a general condition for single-neuron models to be able to learn in a target-based manner and show that this rule is fulfilled in both our model as well as others.

The proof relies on two main assumptions:

- During inference, the apical input changes the neuron activity so that a target level is reached, as different theoretical models proposed Scellier and Bengio (2017); Rao and Ballard (1999); Meulemans et al. (2020).
- During training, the deviation of the apical input at equilibrium $a - a_0$ from the baseline apical activity can be treated as a loss in machine learning. As we saw in Fig. 3, the feedforward error and the amount of required feedback are functionally equivalent.

We will proceed by defining a Lyapunov function for the apical input, and use the invariance of the target rate to insert the learning rules and neuron models into the Lyapunov function.

We start by defining a loss as the amount of apical input with respect to a baseline level. The loss is meant to be used as a Lyapunov function,

$$\mathcal{L}(w) = (a - a^*)^2 \quad (16)$$

where $a^* = 1$ for convenience, and we will consider only strictly positive apical inputs $a \geq 0$. For this to be a Lyapunov function, the function must be strictly positive, as is evident here, and we need to prove that its time derivative, where time is in terms of training iterations, is negative. We start by having the derivative

$$\nabla_w \mathcal{L}(w) = (a - a^*) \Delta a \quad (17)$$

where Δa is the update of the apical input, which is the next thing we need to compute.

In order to be agnostic to the neuron model, we consider a generic neuron dynamics

$$\dot{r}(t) = -r(t) + \varphi \left(\sum_{i \in \text{pre}} w_i r_i(t), a(t) \right) \quad (18)$$

where $\varphi(\cdot, \cdot)$ is a monotonic function that integrates both basal and apical inputs to determine the postsynaptic firing rate, and which covers our neuron model but also others (Rao and Ballard, 1999; Whittington and Bogacz, 2017; Meulemans et al., 2020; Scellier and Bengio, 2017; Sacramento et al., 2018).

We consider the neuron model from Eq. 18 and consider neurons at equilibrium, namely when the feedback has stabilized and the neuron is on its correct firing rate.

$$r = \varphi(z, a) \quad (19)$$

where $z = \sum_{j \in \text{pre}} w_j r_j$ is the presynaptic input.

The target activity is found during inference through a combination of apical and basal inputs, but is crucially always reached as long as the feedback is effective. Thus we can use the inference rate as a fixed point that is maintained even as the apical inputs change and the synapses change.

$$\Delta r = \frac{\partial \varphi(z, a)}{\partial T_{\text{learn}}} = \varphi_a \Delta a + \sum_{i \in \text{pre}} \varphi_z r_i \Delta w_i = 0. \quad (20)$$

where T_{learn} corresponds to temporal variable in learning timescale and φ_a , φ_z are the derivatives of φ with respect to the apical and basal inputs. We can now solve for Δa ,

$$\Delta a = -\frac{\varphi_z}{\varphi_a} \sum_{i \in \text{pre}} r_i \Delta w_i, \quad (21)$$

and plug this into the gradient from Eq. 22,

$$\Delta \mathcal{L}(w) = -\frac{\varphi_z}{\varphi_a} (a - a^*) \sum_{i \in \text{pre}} r_i \Delta w_i, \quad (22)$$

and given that the loss will decrease if the gradient is negative, the condition for learning is reduced to

$$0 \leq \frac{\varphi_z}{\varphi_a} (a - a^*) \sum_{i \in \text{pre}} r_i \Delta w_i \quad (23)$$

for a given neuron dynamics specified by $\varphi(\cdot, \cdot)$ and a given plasticity rule Δw_i .

7.3.1 Our neuron model

In our neuron model,

$$\varphi(z, a) = \phi(z)a \quad (24)$$

with $\phi(\cdot)$ being a rectified linear unit, thus and the plasticity at equilibrium is

$$\Delta w = r_{\text{pre}} r_{\text{post}} (a - a^*), \quad (25)$$

which we can directly plug into Eq. 23

$$0 \leq (a - a^*) \frac{\phi'(z)}{\phi(z)} a \sum_{i \in \text{pre}} r_i r_i \phi(z) (a - a^*) = (a - a^*)^2 \Theta(z) a \sum_{i \in \text{pre}} r_i^2. \quad (26)$$

where $\Theta(\cdot)$ is the step function. Given that $a \geq 0$, the function is strictly positive and, thus, the neuron can use a target-based approach. Notice that in our model there is no gradient when $z < 0$, and the apical input as well as the rates are strictly positive, as one would expect from biological neurons.

7.3.2 Neuron models with additive feedback

To show the similarities and differences between our neuron model and other neuron models used in theoretical models of hierarchical learning in the cortex, we briefly review the neurons that they use and show that they also fulfill the same condition. We will center our works in some well-known target-based models Rao and Ballard (1999); Scellier and Bengio (2017); Meulemans et al. (2020), but the results work also for their successor models.

The models we discussed have additive apical inputs for the somatic firing rate, thus

$$\varphi(z, a) = \phi(z + a) \quad (27)$$

and usually rely on an hyperbolic tangent for the nonlinearity $\phi(\cdot)$, and a baseline apical input $a^* = 0$. The use of additive feedback leads to the simplification

$$\frac{\varphi_z}{\varphi_a} = 1. \quad (28)$$

The same works usually consider a learning rule of the form

$$\Delta w = r_{\text{pre}}(r_{\text{post}} - \bar{r}_{\text{post}}) \quad (29)$$

where \bar{r}_{post} is the postsynaptic neuron firing rate assuming a constant baseline feedback, which in linear models is set to be zero. Given that the activation function ϕ is monotonic, the weight update is given by

$$\Delta w = r_{\text{pre}}\phi'(r_{\in r_{\text{post}} - \bar{r}_{\text{post}}})a \quad (30)$$

where $\phi'(r_{\in r_{\text{post}} - \bar{r}_{\text{post}}}) > 0$ comes from applying the mean value theorem. Plugging this into Eq. 23

$$0 \leq a \sum_{i \in \text{pre}} r_i \Delta w_i = a^2 \sum_{i \in \text{pre}} r_i^2 \phi'(r_{\in r_{\text{post}} - \bar{r}_{\text{post}}}) \quad (31)$$

we see that the same framework applies. Note that such neurons can have positive and negative rates and apical inputs, where the negative values would correspond to firing below a baseline rate.

7.4 Adapting existing architectures

The existing bio-plausible deep learning models that we use are designed with a different type of neurons in mind, and thus we need to make some modifications to make them compatible with our neuron model. In order to insert our neurons into existing architectures, we modified the feedback and the neuron activation functions to make them compatible with our model.

The first key difference between our model and the existing theoretical frameworks is that our apical feedback is multiplicative and strictly positive. As we saw in Eq. 23, this is a requirement for convergence of the learning rule, and to design stable multiplicative feedback loops when the feedback is negative would be difficult. Therefore, we compute our apical feedback as

$$a(t) = 1 + \alpha f(t), \quad (32)$$

where $f(t)$ is the feedback computed by the existing architectures, and $\alpha > 0$ is a constant scalar such that $\alpha f_{\min} \geq -1$ to ensure a positive value for $a(t)$.

Another critical difference between our model and the existing ones regarding neural architectures is that our neuron model cannot have negative rates or apical inputs. This is not only a biological

constraint, but also a computational one. Accepting negative rates would lead to incongruences when combined with multiplicative apical input, as a higher apical input would translate into a reduced (more negative) firing rate.

To ensure positive activities during inference, we used ReLu neurons for both the Predictive Coding and Deep Feedback Control Framework, even though the original works use the hyperbolic tangent. This leaves the neuron models as

$$\dot{r}(t) = -r(t) + \phi(z(t))(1 + \alpha f(t)) = -r(t) + \phi(z) + \phi(z(t))\alpha f(t), \quad (33)$$

where α is very small for Predictive Coding, as expected from the original architecture Whittington and Bogacz (2017). For Equilibrium Propagation, we found that the ReLU activation did not work, so we instead used the hyperbolic tangent. Still, we added a step in between the application of the apical input in order to maintain the qualitative behavior of our neuron model. The main modification is to apply the apical feedback multiplication only after recovering a positive activity by adding the baseline rate,

$$\phi_+(z) = \phi(z) + \beta_\phi, \quad (34)$$

where $\phi(\cdot)$ is the activation function with negative support (here hyperbolic tangent) and $\beta_\phi > \min_x(\phi(x))$. We then recenter the neural activity as

$$\varphi(z, a) = \phi_+(z)a - \beta_\phi, \quad (35)$$

which leaves us with the neuron dynamics

$$\dot{r}(t) = -r(t) + \phi_+(z(t))(1 + \alpha f(t)) - \beta_\phi = -r(t) + \phi(z)(1 + \alpha f(t)) + \beta_\phi \alpha f(t). \quad (36)$$

Crucially, in this network, the sign of $f(t)$ at equilibrium is the same as the sign of the change in firing rate due to the feedback, thus, the learning signal goes in the right direction.

7.5 Separability of neural representations across the hierarchy

To measure the emergence of hierarchical neural representations, we quantify the separability of the neural activity across layers. We do so by considering the average neural activity and spread for a given class measured across all the samples of that class in a given layer,

$$\mu_i^l = \frac{1}{\#\text{class}(i)} \sum_{v \in \text{class}(i)} r^*(i), \quad \sigma_i^l = \frac{1}{\#\text{class}(i)} \sqrt{\sum_{v \in \text{class}(i)} \|r^*(i) - \mu_i^l\|^2}, \quad (37)$$

where i refers to the class and l to the layer. We then take the distance between average neural representations normalized by the spread of neural activity across those two classes, and calculate the average over all pairs of classes,

$$s_l = \frac{2}{N(N-1)} \sum_{i=0}^{C-1} \sum_{j=i+1}^C \frac{\|\mu_i^l - \mu_j^l\|^2}{\sigma_i^l \sigma_j^l} \quad (38)$$

where C is the number of classes, μ_i^l is the average activity for class i on layer l and σ_i^l the spread of the data for a given class. Note that different neuron non-linearities will give different values, thus, if we use hyperbolic tangents or rectified linear units the results will differ.

We also visualized the neural representations using t-SNE (van der Maaten and Hinton, 2008) on each layer. The representations of the testing inputs generate a distribution of points in the two

dominant principal components that become more clustered according to class as in deeper layers, for both MNIST and Fashion-MNIST (see **Supp. Fig. 9**).

7.6 Units and model parameters

The parameters in our model are collected in Table 2.

Parameter	Value	Reference(s)
Duration of AP	1 to 2ms	Gulledge and Stuart (2003)
Refractory period	6ms	Gulledge and Stuart (2003)
Resting membrane potential	-78 to -74 mV	Own experiments
Peak AP	55 to 65mV	Kasper et al. (1994)
Number of spikes in burst	2 to 4 spikes	Own experiments
Duration of EPSP	20 to 30ms	Own experiments
bAP half-width	1 to 4 ms	Stuart et al. (1997)
LTD/LTP threshold	$\theta_{LTP} > \theta_{LTD}$ $\theta_{LTP} \approx 2 \cdot \theta_{LTD}$	Graupner and Brunel (2012), Nevian and Sakmann (2006)
Calcium spike threshold	2.28 (± 0.14) nA	Larkum et al. (1999)
Initiation of plateau potential	5 to 10 ms	Larkum et al. (1999)
Duration of plateau potential	50 to 100 ms	Own experiments
Amplitude of plateau potential	15 mV	Larkum et al. (1999), Own experiments
NMDAR influx vs voltage	$1/(1 + \exp(-0.22 * (x + 49)))$	McRory et al. (2001), Slutsky et al. (2004)
Calcium exp. time constant	81 ± 13 ms	Majewska et al. (2000)
Maximal calcium in synapse	3 a.u. (see NMDAR influx)	n/a
Basal-apical coupling window	20 to 30 ms	Larkum et al. (2004)

Table 2: Hyperparameters of the neuron model with their associated value and references.

8 Supplementary Material

8.1 Somatic Calcium Imaging

While we could not image intracellular calcium dynamics during plasticity induction events, we reproduced typical induction events in a subset of neurons ($n = 7$ neurons, 4 mice) after post-induction EPSP recordings were complete. During these stimulations, we recorded voltage and calcium signals for activity patterns similar to the ones we used for plasticity induction. We found a significant correlation between somatic calcium recordings (derived as $\Delta F/F$ AUC) and PSST-AUC (**Fig. 6B**, $R_{Spearman} = 0.8303$, $p = 0.0029$).

8.2 Apical plasticity

In contrast to our results on basal synapses, we found that for apical synapses neither the plasticity induction AUC ($R_{Spearman} = 0.1049$, $p = 0.7456$, **Fig. 8.2D**) nor the number of APs ($R_{Spearman} = 0.3996$, $p = 0.1982$, **Fig. 8.2E**) are good predictors for changes in synaptic strength. This difference in the predictability of basal versus apical plasticity is also reflected in the finding, that overall changes in basal EPSP amplitudes did not correlate with changes in apical EPSPs ($R_{Spearman} = 0.2308$, $p = 0.4705$, **Fig. 8.2F**).

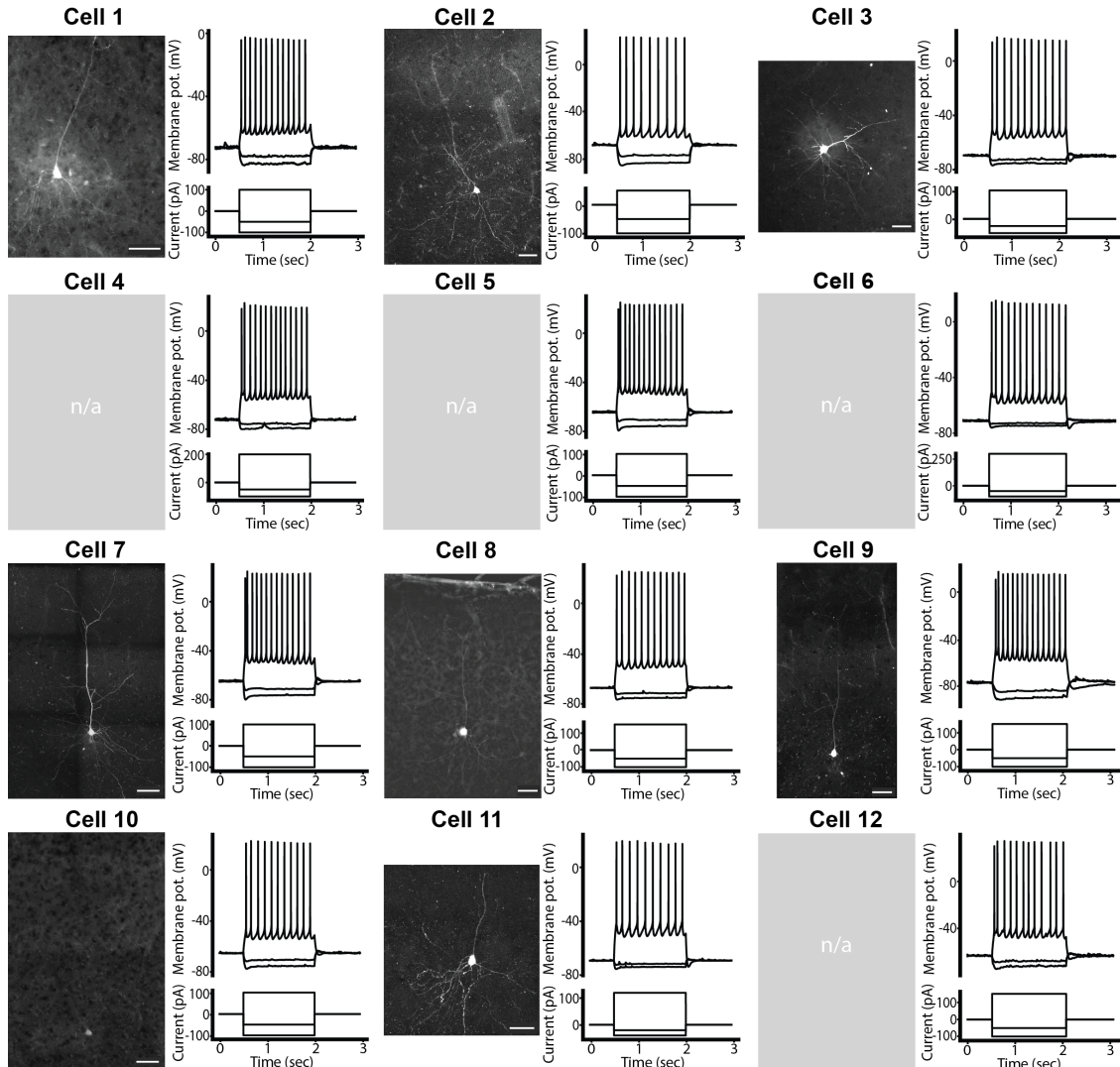


Figure 5: Biocytin-Streptavidin stained neurons (left) and typical hyperpolarizations and action potential trains (right top) induced by negative and positive current injection steps (right bottom) from recorded neurons. For cells 3, 4, 5, and 11, no Biocytin-Streptavidin staining/morphology reconstruction was performed.

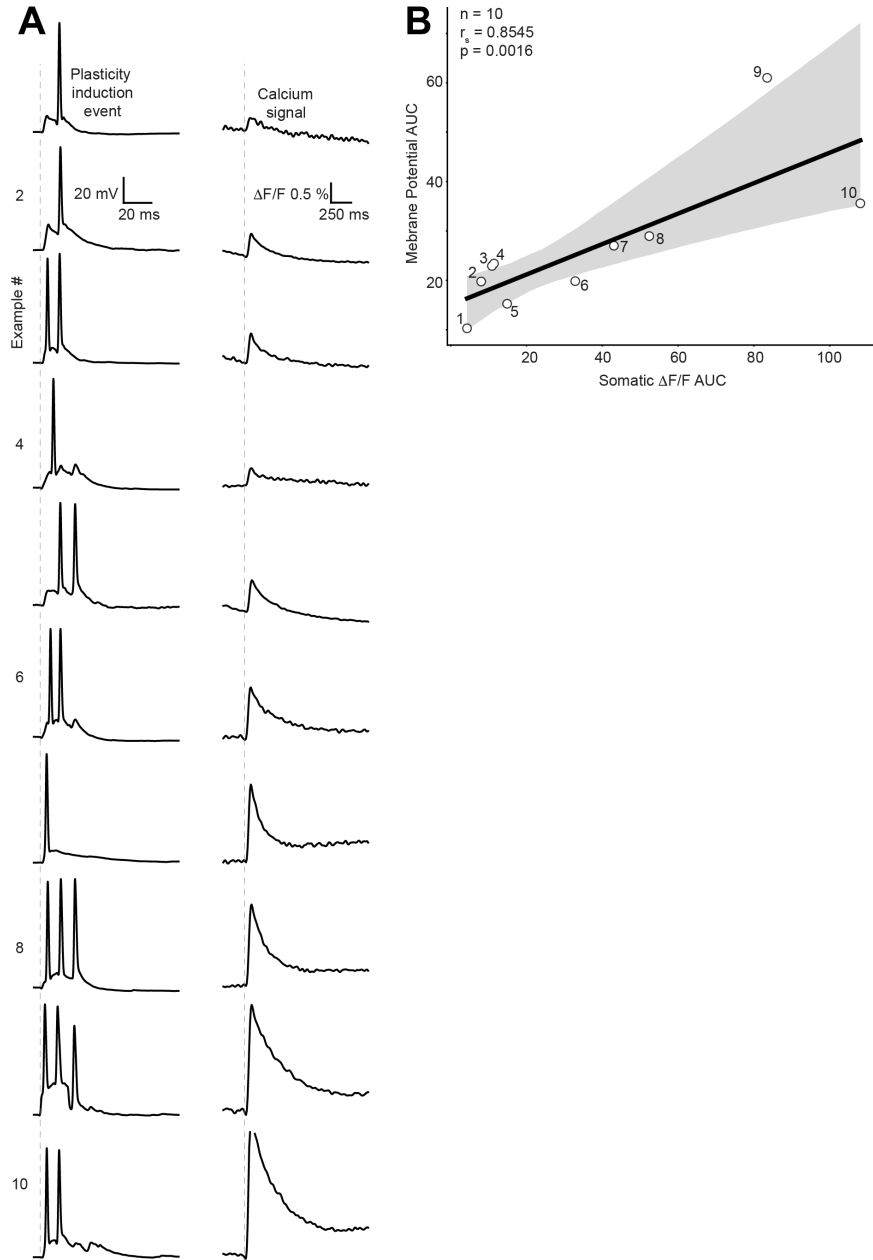


Figure 6: (A) Somatic membrane potential recording during plasticity induction (left) and somatic calcium $\Delta F/F$ during the same event (right). In total, showing events from 10 recordings in 7 neurons (4 mice) from **Fig. 5**. (B) Linear fit of induction event AUCs and somatic calcium signal AUCs showing significant correlation ($n=6$, 10 events total, $r_S=0.8303$, $p=0.0029$)

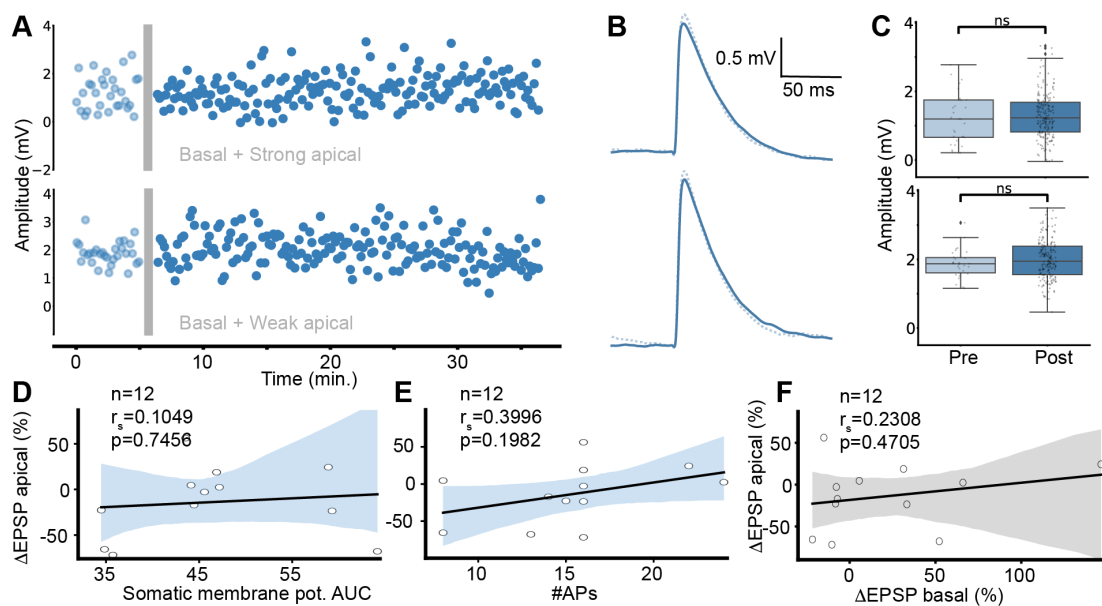


Figure 7: Representative example recordings of EPSP amplitudes during apical stimulation before and after the plasticity induction event (A) EPSP amplitude evolution over time; each dot represents one EPSP pre (light blue) and post (dark blue) plasticity induction event (gray bar). (B) The quantification of EPSPs for two sample cells shows no significant change in EPSP amplitudes. (C, D) Linear correlation analysis between changes in apical EPSP amplitude and somatic membrane potential AUC ((C) $n=12$, $r_s=0.1049$, $p=0.7456$) and number of APs ((D) $n=12$, $r_s=0.3996$, $p=0.1982$), respectively. (E) Correlation analysis of basal and apical ΔEPSP ($n=12$, $r_s=0.3669$, $p=0.2408$).

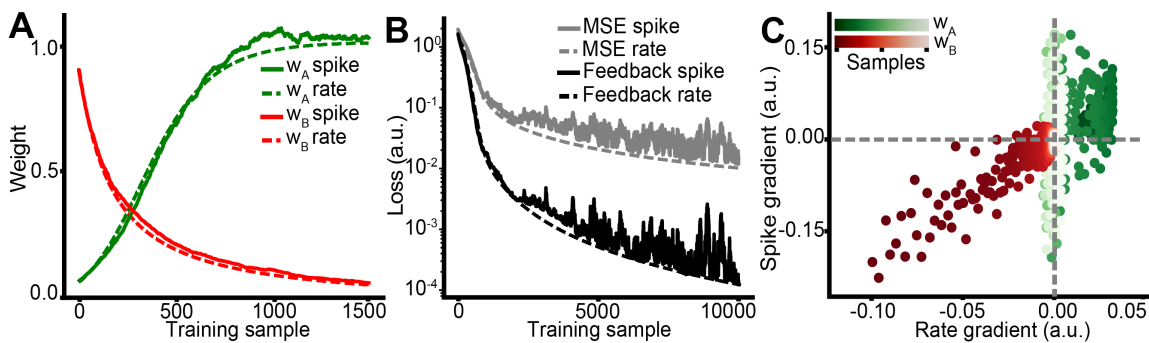


Figure 8: Comparison of spike-based versus rate-based neuron model learning dynamics. (A) Training of the synaptic weights. (B) Evolution of the magnitude of the feedback signal and loss function. (C) Comparison of the change in gradients across the simulation.

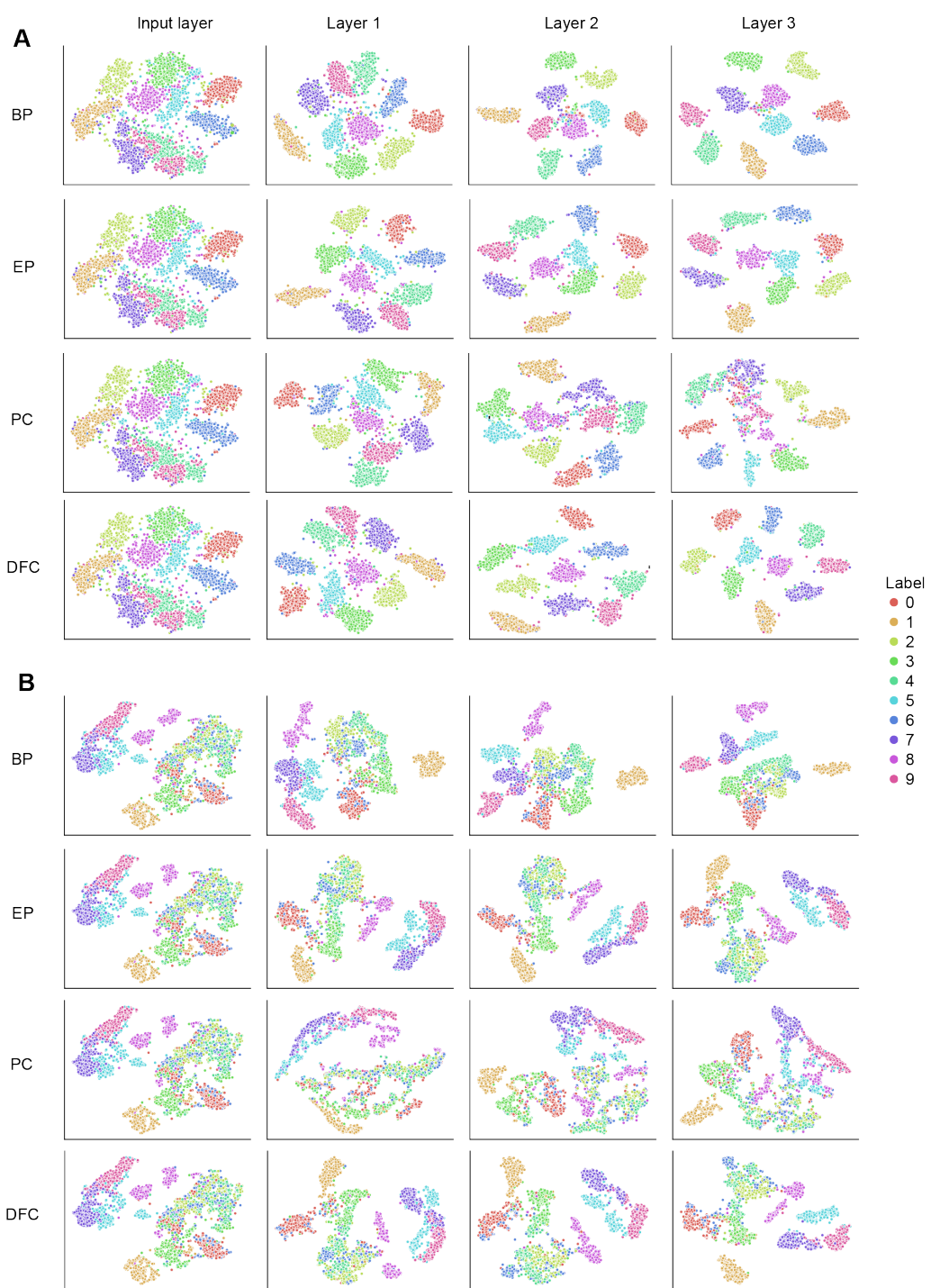


Figure 9: **Visualization of neural representations over layers.** We plot the testing inputs to the network in different layers projected onto the main principal components of the neural activity across layers (columns) and architectures (rows). (A) Corresponds to MNIST and (B) to Fashion-MNIST.